ADVANCED MATERIALS
www.advmat.de

Large-Area Fabrication of Periodic Sub-15 nm-Width Single-Layer Graphene Nanorings

Yusin Pak, Huisu Jeong, Kwang-Ho Lee, Hui Song, Taehyeon Kwon, Jungsu Park, Woojin Park, Mun-Seok Jeong, Takhee Lee, Sunae Seo, and Gun-Young Jung**

Graphene is an allotrope of carbon, the structure of which is a two-dimensional (2D) layer with closely packed hexagonal lattices that resemble a honeycomb.[1] Since the first report of discovering exfoliated graphene in 2004, its value to both fundamental physics and electronics has been demonstrated.[2] The most notable of this work resulted in a Nobel Prize in 2010. Because graphene is a zero-bandgap material,[3] it is inherently infeasible as an active material for field-effect transistors. Therefore, most graphene-related research has been focused on the utilization of its high carrier mobility and the transparency of graphene-based electrodes.[4–7] However, Son et al. theorized that a bandgap opening in graphene could be created by scaling down the width of graphene nanoribbons,[8] and Kim and co-workers[9] and Avouris and co-workers[10] experimentally explored a finite energy gap opening as the width of the graphene ribbons decreased as narrow as 20 nm, arising from electron localization due to impurities and/or localized edge states. Initially, the researchers who investigated the bandgap opening utilized conventional scanning methods such as electron-beam lithography (EBL)[11] and scanning tunnelling microscopy (STM) lithography[12] to fabricate sub-15 nm graphene nanoribbons, despite the fact that these processes were time-consuming and expensive, with a low throughput.

Other innovative nonscanning methods were actively being investigated. Li et al. developed a fabrication technique in which dispersed graphite was centrifuged and broken into pieces of graphene nanoribbons with various ribbon widths.[13] However, the fabrication of aligned graphene nanoribbons with a high density was impossible via this technique. Jiao et al. attempted to cut carbon-nanotube side-walls longitudinally by a simple argon (Ar) plasma etching process,[14] and Bai et al. fabricated graphene nanoribbons by employing silicon nanowires that were in close contact with a graphene sheet as an etching mask, in conjunction with oxygen plasma treatment.[15] The width of graphene nanoribbons is dependent on the diameter of the nanowire and the duration of the etching. However, the fabrication of aligned graphene nanoribbons in a controlled manner over a large surface area remains a challenge.

For practical applications, a dense array of ordered quasi-nanoribbons such as a graphene nanomesh, composed of hexagonally arranged nanopores with graphene necks between the neighboring pores that measure only a few nanometers, was demonstrated by utilization of a nanomesh template generated by a poly(styrene-*block*-methyl methacrylate) (P(S-*b*-MMA)) block copolymer,[16] nanoimprint lithography,[17] and polystyrene nanosphere lithography,[18,19] recently. In the work presented here, we firstly report the fabrication of large-area, high-density, and aligned graphene nanorings (GRNRs) that are sub-15 nm in width, and we confirm their successful fabrication and properties by using various measurement tools such as scanning electron microscopy (SEM), atomic force microscopy (AFM), transmission electron microscopy (TEM), and Raman scattering spectroscopy.

The schematic in **Figure 1** depicts the entire fabrication process of a GRNR array. Three layers comprising a 90 nm-thick imprint resist, 260 nm-thick poly(methyl methacrylate) (PMMA), and 120 nm-thick poly(vinyl alcohol) (PVA) were spin-coated in sequence onto a graphene/SiO_2/Si substrate (Figure 1a). The PVA was utilized as a lift-off layer with water. The PMMA was used to compensate for the low thickness of PVA after spin-coating because the aspect ratio of trench structures is critically important to the successful angle metal deposition, as shown in Figure 1d. Prior to nanoimprint lithography (NIL), an anti-sticking self-assembled monolayer (SAM), which reduced the surface energy of a transparent stamp, was employed to enhance stamp demolding from the imprinted layer.[20] The pillars on the stamp were imprinted into the imprint resist, and the hole patterns were transferred to the under layers by a

Y. Pak,[+] H. Jeong,[+] K. H. Lee, H. Song, W. Park, Prof. G. Y. Jung
School of Materials Science and Engineering
Gwangju Institute of Science and Technology (GIST)
261 Cheomdan-gwagiro
Buk-gu, Gwangju 500-712, Republic of Korea
E-mail: gyjung@gist.ac.kr
T. Kwon, Prof. G. Y. Jung
Department of Nano-biomaterials and Electronics
Gwangju Institute of Science and Technology (GIST)
261 Cheomdan-gwagiro
Buk-gu, Gwangju 500-712, Republic of Korea
J. Park, Dr. M.-S. Jeong
Advanced Photonics Research Institute
Gwangju Institute of Science and Technology (GIST)
261 Cheomdan-gwagiro
Buk-gu, Gwangju 500-712, Republic of Korea
Prof. T. Lee
Department of Physics and Astronomy
Seoul National University
599 Kwan-Ak Ro, Kwan-Ak gu
Seoul 151-747, Republic of Korea
Prof. S. Seo
Department of Physics and Graphene Research Institute
Sejong University
98 Gunja-dong, Kwanggin-gu, Seoul 143-747, Republic of Korea
E-mail: sunaeseo@sejong.ac.kr
[+] These authors contributed equally to this work.

DOI: 10.1002/adma.201202626

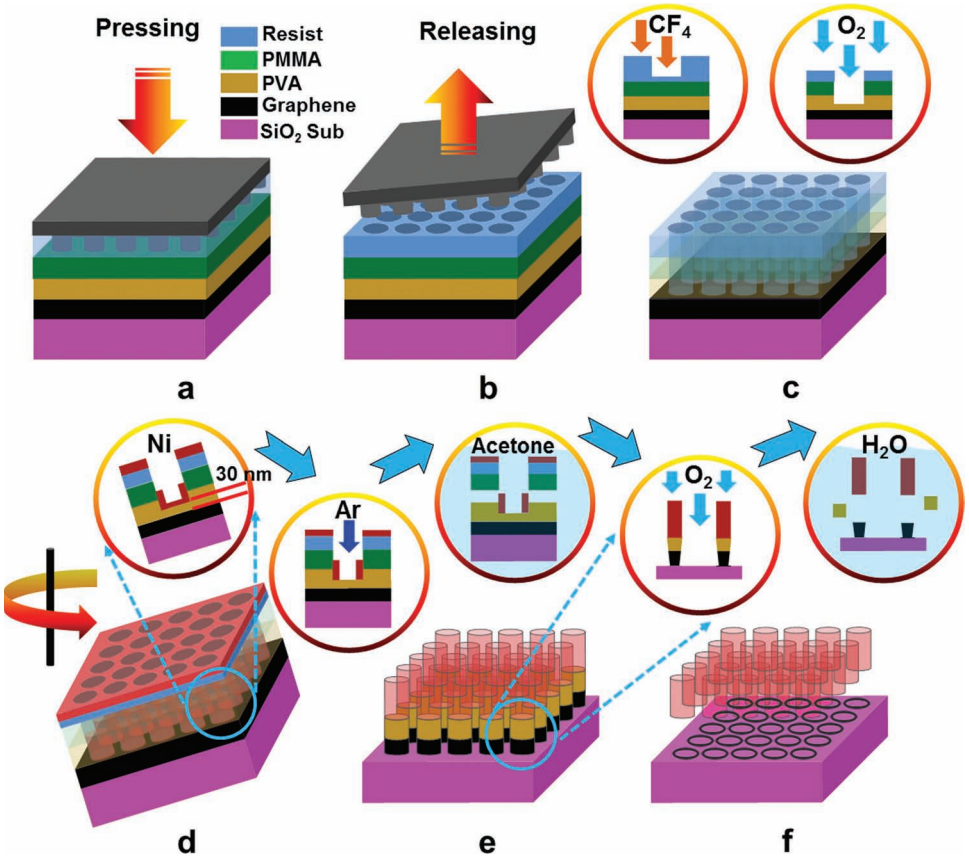

Figure 1. Schematic of the graphene nanoring (GRNR) fabrication process: a) nanoimprint on the imprint resist using an imprint stamp having 120 nm-high pillar features with a diameter of 240 nm at a period of 450 nm. b) Demolding the stamp, leaving behind hole patterns with the same diameter and period as the stamp. c) Etching the residual imprint resist by CF_4 plasma and the subsequent etching of the PMMA/PVA layers by O_2 plasma, deliberately leaving a 30 nm-thick layer of PVA. d) Ni-nanocup structures were produced by glancing-angle deposition on a rotating substrate through a DC-sputtering system. e) Etching of the bottom of Ni nanocups by Ar plasma and subsequent etching of the whole PVA layer and the underlying graphene layer by O_2 plasma, which resulted in a narrower width of the graphene nanorings. f) Ni-nanotube lift-off by dissolving the PVA layer in H_2O.

reactive-ion-etching process using a CF_4 plasma to remove the residual imprint resist and subsequent O_2 plasma treatment to etch both the PMMA and the PVA layers, as shown in Figure 1c. As a result, hole patterns with a diameter of 300 nm and a height of 420 nm were fabricated.

Here, a 30 nm-thick PVA residual layer was deliberately left as a buffer layer, and Ni was deposited by DC sputtering with a sample stage that was rotated at 15 rpm at an angle of 40°, as depicted in Figure 1d. A series of preliminary experiments revealed that an aspect ratio of 1.4 for the trench features is ideal for the angle deposition to consistently generate Ni nanocups (see Supporting Information, Section S1).

To convert the Ni nanocups shown in Figure 1d into the Ni nanotubes shown in the middle of Figure 1d,e, the bottoms of the Ni nanocups were extracted by Ar plasma after the angle deposition. A controlled etching process was performed to etch only the Ni bottoms and expose the PVA buffer layer. Without the PVA buffer layer, the inductively enhanced Ar plasma, at a power of 300 W, etched the bottom of the Ni nanocups anisotropically and destroyed the graphene layer underneath. Furthermore, back-scattered Ar ions with a high energy at the substrate surface could attack the thin sidewalls of the as-made Ni nanotubes, thereby causing the nanotube walls to collapse. The substrate was then submerged in acetone to remove the Ni/imprint resin/PMMA layers, which left only the PVA layer, in which the Ni nanotubes were embedded (Figure 1e). Finally, O_2 plasma was used to remove both the PVA layer and the graphene underneath. Because the inner portion of a Ni nanotube has a much thinner PVA layer, over-etching was conducted to generate undercuts in the PVA layer under the Ni nanotubes, which resulted in a reduction of the GRNR width, as depicted in the middle of Figure 1e,f. Because of the undercuts, the nanoring width was reduced to sub-15 nm, on average, from the 20 nm-wide Ni sidewalls. Finally, the sample was submerged in water to lift-off the PVA layer and the Ni on top of it. The defined GRNRs were then annealed in a chemical vapor deposition (CVD) system at 400 °C for 1 h to remove organic debris and moisture (see the Experimental Section for more details).

Figure 2a shows the polymeric template, having the imprinted holes with a diameter of 240 nm at a 450 nm pitch; Figure 2b shows the resultant Ni-nanotube array obtained after the Ar plasma etching/acetone soaking/O_2 plasma steps depicted in Figure 1e. The Ni nanotubes were created in the entire imprinted area of nearly 3 cm × 3 cm. The diameter of

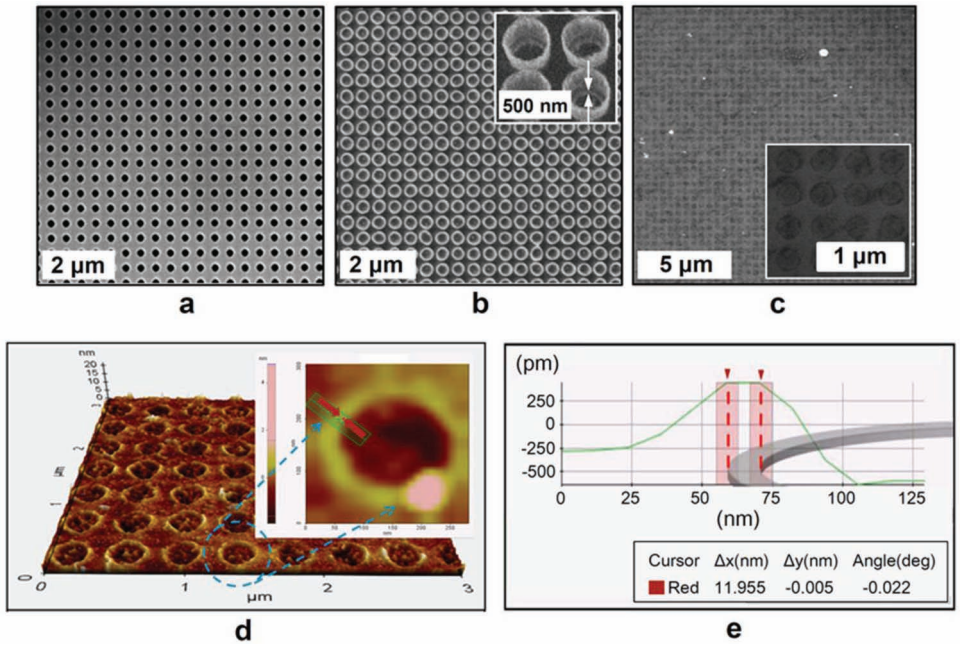

Figure 2. SEM and AFM images of a major step of the GRNR fabrication process. a) SEM image of nanoimprinted hole patterns with a 240 nm diameter at a 450 nm period. b) SEM image of the Ni-nanotube array with a 300 nm diameter and the magnified tilt-view of four nanotubes showing that the Ni-nanotube bottom was etched away by the anisotropic Ar etching (inset). c) SEM image of GRNRs array for a 15 μm × 15 μm area (the inset is a magnified image covering 16 GRNRs). d) AFM image of the GRNR array. e) Surface profile of one GRNR. The 12 nm-wide and 0.7 nm-thick graphene nanorings arrays were generated in a controlled manner.

the Ni-nanotube array was expanded from 240 nm of polymeric holes to 300 nm during the pattern transfer by dry-etching. The height and width of the Ni nanotubes were approximately 250 nm and 20 nm, respectively. In the inset of Figure 2b, four Ni nanotubes and the trace of the nanocup bottom edges (between the white arrows) demonstrate that the plasma process used to convert the nanocups to nanotubes was feasible without destruction of the basic nanotube array. Figure 2c is an SEM image of GRNRs, taken for a 15 μm × 15 μm area, and a magnified SEM image covering 16 GRNRs is inset. The final GRNRs are produced in half of the total substrate area of 9 cm^2, demonstrating the feasibility of wafer-scale GRNR fabrication. Among them, statistically, 30% of GRNRs were found to have a perfect ring structure with a width of sub-15 nm, but the rest of the GRNRs were broken locally along the perimeter.

The AFM image in Figure 2d shows the aligned GRNRs that remain after the water lift-off and the thermal annealing. The surface profile between the two red arrows in the inset of Figure 2d, which is a high-resolution AFM image of a graphene nanoring, demonstrates that the as-made GRNR had a thickness of less than 0.7 nm, which indicates that near-single-layer graphene nanorings were generated. Taking into consideration that the AFM was scanned in noncontact mode, the flat region of 12 nm represented by the two red triangles (Figure 2e) is considered to be the GRNR width. The rough SiO_2 surface (especially the inside area of the GRNRs) was attributed to the bombardment of O_2 ions. As found in the surface profile, a difference exists between the inside and outside depths around the GRNR: 0.7 nm vs. 1 nm, respectively. The difference in depth originated from the initial difference in thickness of the PVA layers between the two regions, which were removed by anisotropic O_2 plasma etching. The inside, shallow PVA layer was first etched away, and the exposed SiO_2 surface was then bombarded by the ions, which resulted in a rougher surface and a greater depth.

Micro-Raman scattering was measured to observe the changes in the graphene layer during the fabrication process. A Nd:YVO_4 diode-pumped solid-state laser with a wavelength of 532 nm was used at a power of 14 mW and focused onto the sample using a micro-objective lens with a spot diameter of 1 μm. Finally, the Raman scattering signal was dispersed and detected by a triple monochromator attached to a charge-coupled device (CCD) (ACTON TRIVISTA) with a spectral resolution of 0.2 cm^{-1}. **Figure 3**a and 3b show the Raman scattering spectra of the pristine graphene and the GRNR, respectively. The corresponding Raman peak positions are summarized in **Table 1**. From the full-width at half-maximum (FWHM) of the 2D band (29.5 cm^{-1}) of the pristine graphene (inset of Figure 3a), we conclude that the pristine graphene used in this study was very close to being single-layer graphene (SLG).[21] After the fabrication of the GRNRs, although the FWHM of the 2D band was broadened to 33.5 cm^{-1} (inset of Figure 3b), the

Table 1. Representative Raman peaks and ratios for SLG and GRNRs.

Types	D [cm^{-1}]	G [cm^{-1}]	2D [cm^{-1}]	I_D/I_G	I_{2D}/I_G	2D FWHM [cm^{-1}]
SLG	1341.3	1588.1	2684.5	0.2	1.7	29.5
GRNR	1351.7	1589.1	2687.1	0.6	1.2	33.5

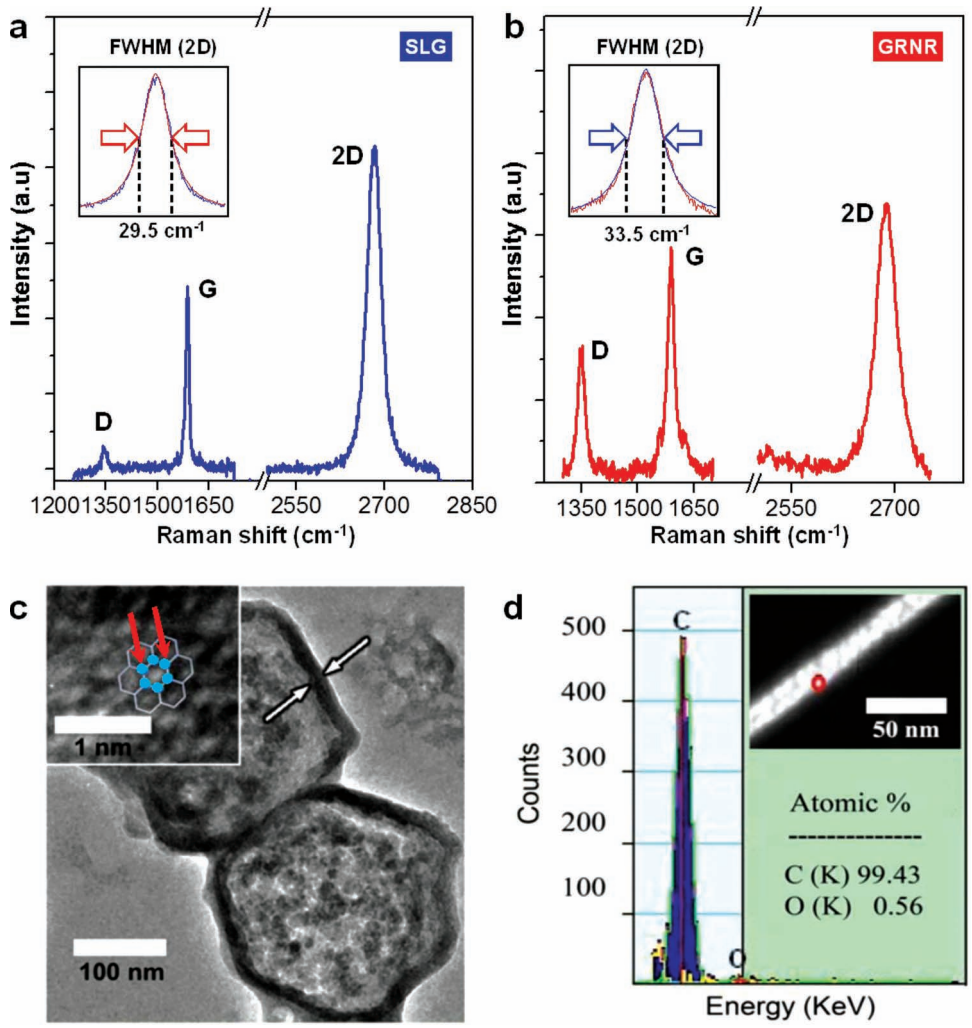

Figure 3. Raman scattering spectra of: a) the pristine graphene with a 2D band FWHM of 29. 5 cm^{-1}, indicating single-layer graphene (SLG), and b) graphene nanorings (GRNRs) with blue-shifted G, D, and 2D bands, compared with those of the pristine graphene. c) A TEM image of two GRNRs; the HR-TEM image (inset) was taken at the ring, and shows a hexagonal distribution of carbon atoms. d) EDS analysis of the graphene rings demonstrated a carbon quantity of above 99%. These two results strongly support the fabrication of GRNRs.

GRNRs remained as SLG. Moreover, the G, D, and 2D bands of the GRNRs were blue-shifted from those of SLG. The blue-shift of the G and D bands may have been caused by a hole-doping effect due to H_2O during the fabrication process.[22] The increase in the graphene edges during the fabrication of the GRNRs is considered to be the primary reason for the increase in the I_D/I_G ratio.[23]

TEM analysis was also performed to confirm the fabrication of GRNRs. For the specimen preparation, a few drops of a buffered oxide etchant (BOE) were added on top of the sample to etch the silicon dioxide and float the GRNRs, and then the sample was immersed into isopropyl alcohol under a sonication ambient. The as-made solution was dropped onto a Cu grid and naturally dried in the air (see Supporting Information, Section S2). Figure 3c shows a TEM image of two GRNRs. However, it shows the unavoidable generation of a multistack of GRNRs due to the van der Waals interaction between the GRNRs in the solution phase. It was also hard to get a perfect ring shape because the capillary force exerted by the solution sitting inside the GRNR transformed the original shape of the GRNRs during the natural air-drying. Furthermore, the shape was distorted when exposed to the electron currents during imaging. The high-resolution (HR) TEM image (inset of Figure 3c) was taken from the graphene ring between the white arrows in Figure 3c, and shows a hexagonal distribution of carbon atoms. The six hexagonally arranged blue dots represent carbon atoms of an in-plane unit cell with a lattice constant of 0.25 nm (between the red arrows in the inset of Figure 3c) which nearly corresponds to the previously reported value.[24] The energy-dispersion spectroscopy (EDS) analysis of Figure 3d revealed a 99.43% carbon signal. Both the HR-TEM image and the EDS results also strongly support the fabrication of GRNRs.

Nanoscale top electrodes were defined by NIL and a subsequent lift-off process. For the top electrode contacts, 3 nm-thick Ti and 40 nm-thick Au were successively deposited using an electron-beam evaporator with a deposition rate of 0.2 nm s^{-1} at 1×10^{-6} Torr. **Figure 4**a shows the top electrodes, in which ten 100 nm-wide wires were aligned to the underlying GRNRs

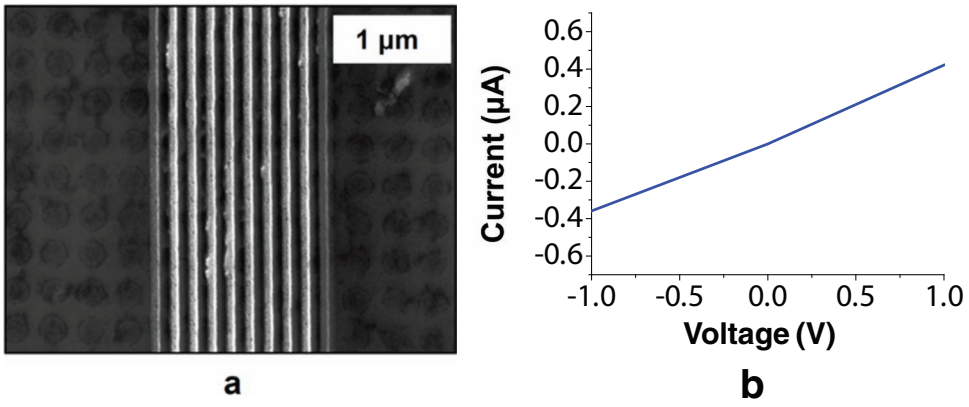

Figure 4. a) 10 parallel, gold, top electrodes with a linewidth of 100 nm at a 200 nm pitch on top of the GRNRs. b) The current–voltage characteristics of the GRNRs, measured between the two neighboring top electrodes.

at a 100 nm half-pitch scale on the 300 nm-thick SiO_2 dielectric layer. If the nanowires are well aligned to the GRNR array, nearly seventy GRNRs can be placed beneath the two neighboring nanowires with a length of 30 μm. The current (I) versus voltage (V) characteristics in Figure 4b, measured between the two neighboring top electrodes, show a current level of 10^{-7} A at ±1 V, indicating that the GRNRs were electronically conductive and physically continuous.

In summary, we have fabricated single-layer GRNRs with a sub-15 nm width on a large area of 9 cm^2, that could accommodate an imprint stamp size via NIL, by a combination of the angle-deposition method and sophisticated plasma-etching processes. Raman scattering measurements verified that the fabricated GRNRs were still intact. In addition, AFM analysis demonstrated that the sub-15 nm-wide GRNRs were fabricated with a high fidelity, and the TEM and EDS results strongly support the existence of GRNRs. This large-area graphene patterning technique at sub-15 nm has the potential to contribute to future integrated electronics based on single-layer graphene.

Experimental Section

Preparation of the Imprint Stamp: The imprint stamp was fabricated by using 325 nm He-Cd laser-interference lithography[25] and subsequent dry-etching process (see Supporting Information, Section S3). Pillars were generated with a diameter of 240 nm at a 450 nm period. Prior to imprinting, an antisticking self-assembled monolayer (SAM) was deposited onto the stamp surface to assist demolding from the imprinted resist.[20]

Single-Layer-Graphene Transfer onto a SiO_2 Substrate: The substrate for the graphene growth was prepared by deposition of a Cu/Ni thin film with a total thickness of 300 nm on a SiO_2 (300 nm)/Si wafer using electron-beam evaporation, and was then placed in an inductively coupled-plasma chemical vapor deposition (ICP-CVD) chamber. The substrate temperature was ramped from room temperature to 650 °C at a base pressure of 5×10^{-7} Torr. A radio-frequency (RF) plasma source was applied to clean the wafer surface under flowing hydrogen, and graphene was grown for 3 min in an Ar + C_2H_2 gas mixture with a plasma power of 100 W.[26]

After cooling, the CVD-grown graphene was transferred to another SiO_2 (300 nm)/Si wafer. For this purpose, we spin-coated PMMA as a protective layer on the grown graphene layer and attached a pressure-sensitive adhesive UV-tape as an adhesive layer across the entire growth wafer. After the UV tape/PMMA/graphene/metal layers were mechanically peeled from the initial SiO_2 layer, they were placed in an $FeCl_3$ solution to etch the metal layers. We then displaced UV tape/PMMA/graphene onto the target SiO_2 host wafer and removed the UV-tape and PMMA layer in an organic bath. Finally, the substrate was cleaned in isopropyl alcohol (IPA).

Nanoimprint Lithography, Metal Deposition, and Pattern Transfer to Graphene: Prior to NIL, PVA and PMMA were sequentially spin-coated as under-layers under the following conditions: PVA (4% diluted, 30 s, 4000 rpm, baked at 100 °C for 20 s); PMMA (4% diluted, 40 s, 2000 rpm, baked at 100 °C for 2 min). The imprint resist, which was a mixture of UV-curable polydimethylsiloxane material (Gelest, 87%), a radical initiator (Irgacure 184, Ciba, 3%), and a cross-linker (ethylene glycol dimethacrylate, Aldrich, 10%), was then spin-coated at 6500 rpm for 150 s and subjected to imprinting at a pressure of 5.2×10^3 Torr under UV irradiation for 10 min, with a transparent stamp having pillar features. After demolding, the trenches were treated with CF_4 plasma (50 sccm, 20 mTorr, 20 W, 30 s) to remove the residual layer at the trenches, and subsequently treated with O_2 plasma (50 sccm, 20 mTorr, 20 W, 210 s) to transfer the imprinted patterns to the under-layers of PMMA and PVA. Ni was then deposited with a deposition rate of 0.2 nm s^{-1} at 10^{-6} Torr by DC sputtering on a sample stage rotated at 15 rpm at an angle of 45°.

The Ni nanocups were converted into Ni nanotubes by highly energetic anisotropic Ar-ion bombardment on the bottoms of the Ni nanocups for 20 s under conditions of 50 sccm, 100 W of the bottom field, 300 W of the top field, and 10 mTorr. The PMMA layer was then lifted off by soaking for a few seconds in acetone under a mild sonication. Only the Ni nanotubes surrounded by the PVA layer remained. The sidewall width of the Ni nanotubes was transferred to the SLG using O_2 plasma to etch the entire PVA layer and the underlying graphene for 100 s under conditions of 50 sccm, 25 W, and 20 mTorr. The sample was then submerged in water to lift off the PVA layer under the Ni nanotubes, which resulted in only GRNR patterns. After the sample was cleaned with acetone/IPA for few seconds, thermal annealing was performed at 400 °C for 1 h in a CVD system under the following conditions: 100 sccm of H_2, 10 sccm of Ar, and 4 Torr.

Supporting Information

Supporting Information is available from the Wiley Online Library or from the author.

Acknowledgements

This work was partially supported by the Basic Research Program through the National Research Foundation of Korea (NRF)

(No. R15-2008-006-03002-0, CLEA, NCRC) and the World Class University Program (WCU) (No. R31-2008-000-10026-0) at GIST funded by the Ministry of Education, Science and Technology (MEST). The program for integrated molecular systems and the project for practical R&D grants at GIST also supported this research. S.S. thanks the Priority Research Centers Program (2012-0005859). M.-S.J. was supported by the Nano R&D program (2007-02939).

Received: June 29, 2012
Revised: September 20, 2012
Published online: October 29, 2012

[1] A. K. Geim, K. S. Novoselov, *Nat. Mater.* **2007**, *6*, 183.
[2] K. S. Novoselov, A. K. Geim, S. V. Morozov, D. Jiang, Y. Zhang, S. V. Dubonos, I. V. Grigorieva, A. A. Firsov, *Science* **2004**, *6*, 666.
[3] K. S. Novoselov, A. K. Geim, S. V. Morozov, D. Jiang, M. I. Katsnelson, I. V. Grigorieva, S. V. Dubonos, A. A. Firsov, *Nature* **2005**, *438*, 197.
[4] H. A. Becerril, J. Mao, Z. Liu, R. M. Stoltenberg, Z. Bao, Y. Chen, *ACS Nano* **2008**, *2*, 463.
[5] X. Wang, L. Zhi, K. Mullen, *Nano Lett.* **2008**, *8*, 323.
[6] C. A. Di, D. Wei, G. Yu, Y. Liu, Y. Guo, D. Zhu, *Adv. Mater.* **2008**, *20*, 3289.
[7] F. Bonaccorso, Z. Sun, T. Hasan, A. C. Ferrari, *Nat. Photonics* **2010**, *4*, 611.
[8] Y.-W. Son, M. L. Cohen, S. G. Louie, *Nature* **2006**, *444*, 347.
[9] M. Y. Han, B. Ozyilmaz, Y. Zhang, P. Kim, *Phys. Rev. Lett.* **2007**, *98*, 206806.
[10] Z. Chen, Y.-M. Lin, M. J. Rooks, P. Avouris, *Physica E.* **2007**, *40*, 228.
[11] B. Ozyilmaz, P. Jarillo-Herrero, D. Efetov, P. Kim, *Appl. Phys. Lett.* **2007**, *91*, 192107.
[12] L. Tapaszto, G. Dobrik, P. Lambin, L. P. Biro, *Nat. Nanotechol.* **2008**, *3*, 397.
[13] X. Li, X. Wang, L. Zhang, S. W. Lee, H. J. Dai, *Science* **2008**, *319*, 1229.
[14] L. Jiao, L. Zhang, X. Wang, G. Diankov, H. J. Dai, *Nature* **2009**, *458*, 877.
[15] J. Bai, X. Duan, Y. Huang, *Nano Lett.* **2009**, *9*, 2083.
[16] J. Bai, X. Zhong, S. Jiang, Y. Huang, *Nat. Nanotechnol.* **2010**, *5*, 190.
[17] X. Liang, Y. S. Jung, S. Wu, A. Ismach, D. L. Olynic, S. Cabrini, J. Bokor, *Nano Lett.* **2010**, *10*, 2454.
[18] L. Liu, Y. Zhang, W. Wang, C. Gu, X. Bai, E. Wang, *Adv. Mater.* **2011**, *23*, 1246.
[19] N. S. Safron, A. S. Brewer, M. S. Arnold, *Small* **2011**, *7*, 492.
[20] G.-Y. Jung, Z. Li, W. Wu, Y. Chen, D. L. Olynick, S.-Y. Wang, W. M. Tong, R. S. Williams, *Langmuir* **2005**, *21*, 1158.
[21] Y. Y. Wang, Z. H. Ni, T. Yu, Z. X. Shen, H. M. Wang, A. T. S. Wee, *J. Phys. Chem.* **2008**, *112*, 10637.
[22] I. Gierz, C. Riedl, U. Starke, C. R. Ast, K. Kern, *Nano Lett.* **2008**, *8*, 4603.
[23] B. Krauss, P. Nemes-Incze, V. Skakalova, L. P. Biro, K. V. Klitzing, J. H. Smet, *Nano Lett.* **2010**, *10*, 4544.
[24] S. Reich, J. Maultzsch, C. Thomsen, *Phys. Rev. B* **2002**, *66*, 035412.
[25] B. Y. Choi, Y. Pak, K.-S. Kim, K. H. Lee, G.-Y. Jung, *Nanoscale Res. Lett.* **2011**, *6*, 449.
[26] J. Lee, H.-J. Chung, J. Lee, H. Shin, J. Heo, H. Yang, S.-H. Lee, S. Seo, J. Shin, U.-I. Chung, I. Yoo, K. Kim, in *2010 IEEE Int. Electron Devices Meeting (IEDM)*, **2010**, pp. 568–571.